The two active glutamates of the plant stress sensor PsbS contribute non-equivalently to its pH-activated molecular response mechanism

Maithili Krishnan[1¶], Patrick E. Konold[2¶], John T.M. Kennis[2,*], Anjali Pandit[1,*]

[1] Dept. of Solid-State NMR, Leiden Inst. of Chemistry, Leiden University, Einsteinweg 55, 2300 RA, Leiden, The Netherlands

[2]Department of Physics and Astronomy, Faculty of Sciences, Vrije Universiteit, De Boelelaan 1081, 1081HV Amsterdam, The Netherlands

[¶]these authors contributed equally

ABSTRACT

The membrane protein Photosystem II subunit S (PsbS) is a pH sensor that plays an essential role in signaling light stress in plants to prevent photo oxidation and generation of detrimental reactive species. PsbS detects thylakoid lumen acidification in excess light conditions via two glutamates facing the lumen, however, its molecular mechanism for activation has remained elusive. We performed an infrared and 2-dimensional infrared spectroscopic analysis of wild type *Physcomitrella patens* PsbS and of mutants in which the active glutamates have been replaced: E71Q, E176Q (the equivalent of E69Q and E173Q in *spinach* PsbS) and the double mutant E71Q/E176Q. We discovered that E71 exerts allosteric control of PsbS dimerization, while E176 is essential for the secondary structural response to low pH. Based on our results, we propose a molecular pH response mechanism that involves re-positioning of the amphipathic short helix facing the lumen, whereby it moves from the aqueous phase into the hydrophobic membrane phase upon lowering the pH. This structural mechanism may be a shared motif of protein molecular

switches of the light-harvesting family and its elucidation could open new routes for crops engineering to improve photosynthetic production of biomass.

Introduction

Photosynthetic efficiency is tightly coupled with plant fitness under fluctuating environmental conditions, which is prerequisite for survival in a changing global climate. Key to vitality is a continuous balance between light excitation and substrate availability, preventing overload of the electron transfer chain and formation of lethal reactive oxygen species. Overload of the electron-transfer chain in excess light causes acidification of the chloroplast luminal compartments. This provokes a kinetic switch of the photosynthetic antenna into a dimmer state, where excitations are rapidly quenched by a process called Non-Photochemical Quenching (NPQ) [1,2]. Whereas the photo protective feedback response is beneficial for plant fitness, large part of the absorbed solar energy is dissipated during the photo protective state and its transient recovery.

The heart of the photo protective mechanism lies in the molecular response to ΔpH. The protein PsbS was identified as gene product required for NPQ activation in plants [3]. PsbS is a member of the greater LHC superfamily, but in contrast to all other proteins in this family, it does not specifically bind any chlorophyll or xanthophyll pigments [4,5]. PsbS acts as a molecular pH-sensor that senses thylakoid lumen acidification and transfers the signal to the antenna, enabling a switch into a photoprotective state via antenna-photosystem rearrangements that involve changes in protein-protein or pigment-protein molecular interactions [6-11] [11-17]. PsbS activation involves two lumen-faced glutamate (Glu0 residues and may involve a monomerization step [18], although the recently resolved low-pH X-ray structure is a PsbS dimer [19]. Each PsbS monomer consists of four transmembrane (TM) helices and two amphipatic short helix stretches (H1 and H2) at the luminal side and the structure display an overall pseudo-two-fold symmetry (see Fig. 1). On basis of the high sequence identity between the two halves of the protein together with the NPQ responses of site-directed Glu mutants *in vivo*, the two active Glu, E69 and E173

in *spinach* PsbS were proposed to be equivalent in their response to pH: the mutants E69Q and E173Q both exhibited significantly reduced the NPQ responses, while the double mutant E69Q/E173Q did not show any appreciable NPQ response [20]. So far, the molecular response mechanism of PsbS activation has remained elusive and could not be revealed by crystallography.

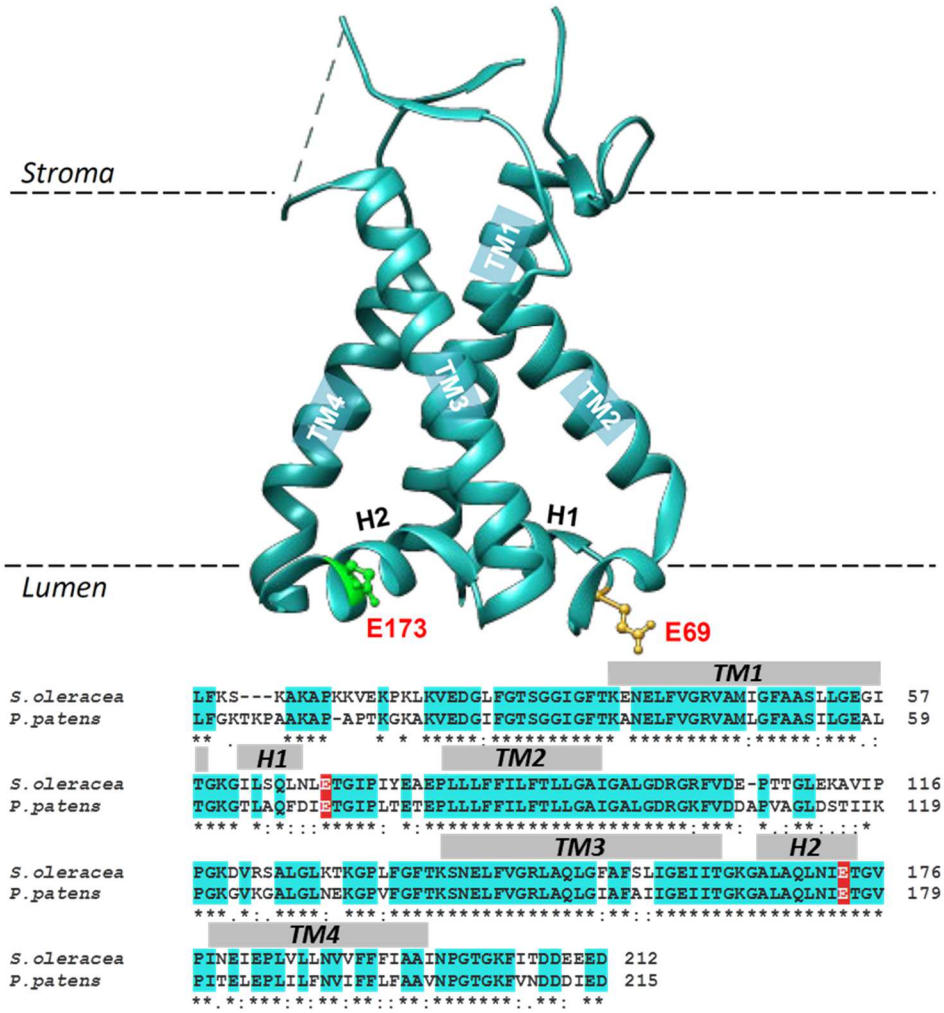

Figure 1. Structure of *spinach* PsbS (*PDB-ID 4RI2* [19]), highlighting the active Glu (E69 in yellow and E173 in green). Part of the stromal loop between TM2 and TM3 is not resolved in the X-ray structure (dashed line indicates the two connecting sites). The sequence alignment bellows shows the amino acid sequences of *spinach* (*S. oleracea*) and *patens* (*P. patens*) PsbS, highlighting the two active Glu in red.

PsbS not only is essential for plant photoprotection, but also offers perspectives for targeted crop engineering. A recent study demonstrated that ~15% increase of crop yield could be achieved in engineered Tobacco plants with increased levels of PsbS that had faster photo protective response kinetics [21]. Moreover, raising PsbS levels was shown to increase water use efficiency of tobacco plants [22] and canopy radiation use efficiency in rice plants [23].

We recently introduced strategies for large-scale recombinant production, refolding and dimerization of PsbS for structural characterization [24]. In this article, we compare the pH-dependent structure and dynamics of wild type (WT) PsbS from *Physcomitrella patens* to that of site-directed glutamate mutants that were shown to have impaired activity *in vivo,* by which we identify the pH-dependent response mechanism of PsbS.

Results

Three *P. patens* PsbS mutants were constructed, in which the active Glu were mutated to Gln: E71Q, E176Q (the equivalent of E69Q and E173Q in *spinach* PsbS) and the double mutant E71Q/E176Q, further denoted as M1 (E71Q), M2 (E176Q) and M3 (E71Q/E176Q). The two active Glu residues E71 and E176 are further denoted as Glu-1 and Glu-2. In plants, single mutations of either of the two conserved Glu resulted in reduced NPQ activity, while double mutants exhibit almost complete abolishment of NPQ [20]. The wild type PsbS and M1, M2 and M3 mutants were refolded in *n*-Dodecylphosphocholine (FC-12) detergent micelles as described earlier for the wild type [24] and protein-detergent solutions were equilibrated at pH 7.5 or pH 5.0 in 100mM sodium phosphate buffer (pH 7.5) or 100mM sodium acetate buffer (pH 5.0).

Dimer/monomer content in wild-type and mutant PsbS as a function of pH

Fig. 2 presents a Sodium Dodecyl Sulfate (SDS)-page gel electrophoresis analysis of the four samples under pH 7.5 and pH 5.0 conditions. Although denaturing buffer conditions were used, dimer bands are

observed, which are in agreement with previous studies that PsbS can form strong dimers that resist gel denaturation [18,24]. Standard SDS-page using denaturing gel conditions involves a boiling step, which was also omitted here to test the effect on PsbS dimer stability. The figure shows that all the mutants have lower dimer content than the wild type, whereby the dimer contents vary for the different mutants in the order: dimer content M1 < M3 < M2. Strikingly, mutation of Glu-1 results in the complete absence of dimers on gel, indicating a strong effect of dimer destabilization.

The dimer contents on gel were somewhat increased for the wild type at low-pH conditions. The fact that PsbS can form dimers at low and neutral pH has already been confirmed by previous work [24] and agrees with the low-pH crystal structure that is a PsbS dimer [19].

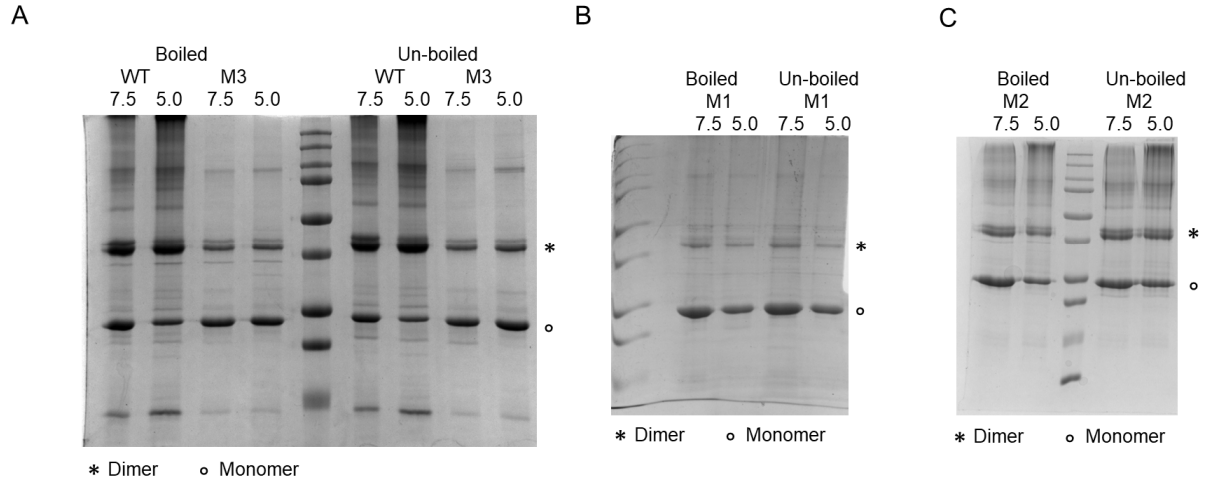

Figure 2. SDS-page analysis of PsbS at pH 7.5 and pH 5.0 conditions. A: Wild-type PsbS and E71Q/E176Q mutant M3; B: E71Q mutant M1 and C: E176Q mutant M2.

Protonation states of WT and mutant PsbS assessed by solid-state NMR

To reveal PsbS protonation states at pH 7.5 and 5.0 conditions, uniformly isotope labeled *U*-^{13}C-^{15}N wild type PsbS and *U*-^{13}C-^{15}N M3 were produced for analysis by solid-state Magic-Angle Spinning (MAS) NMR spectroscopy. Fig. 3 presents the 1D ^{13}C MAS-NMR spectra of the two samples. Direct ^{13}C polarization MAS NMR was applied because the dimensions of PsbS in detergent micelles are such that

rotational correlation dynamics averages dipolar nuclear couplings, reducing the efficiency of cross-polarization based MAS NMR, while the sizes are too large for detection of rigid protein sites by solution NMR. At pH 7.5, two clear peaks are observed of deprotonated Glu and Asp carboxylic-acid side chains, both for the wild type and M3 (Fig. 3A and C). At pH 5.0, these peaks are shifted upfield and overlap with the large ^{13}C' peak centered at 175 ppm of the protein carbonyls, indicating that all the titratable Asp and Glu residues are protonated at pH 5.0 (Fig. 3B and D). The shape of the carbonyl ^{13}C' band of the M3 mutant differs from the wild type, both at pH 7.5 and at pH 5.0 (Fig. 3C and D, respectively), which indicates that there are differences between the secondary structure of the wild type and the M3 mutant. Carbonyl ^{13}C NMR chemical shift resonances of α-helical amino acids are shifted downfield with respect to those of random coil amino acids, while the carbonyl resonances of β-sheet amino acids are shifted upfield [25]. The carbonyl NMR spectra of M3 contain more NMR signal between 172-175 ppm than the wild type, both at pH 7.5 and pH 5.0, which suggests that the secondary structure of the M3 mutant has more coil or sheet contributions.

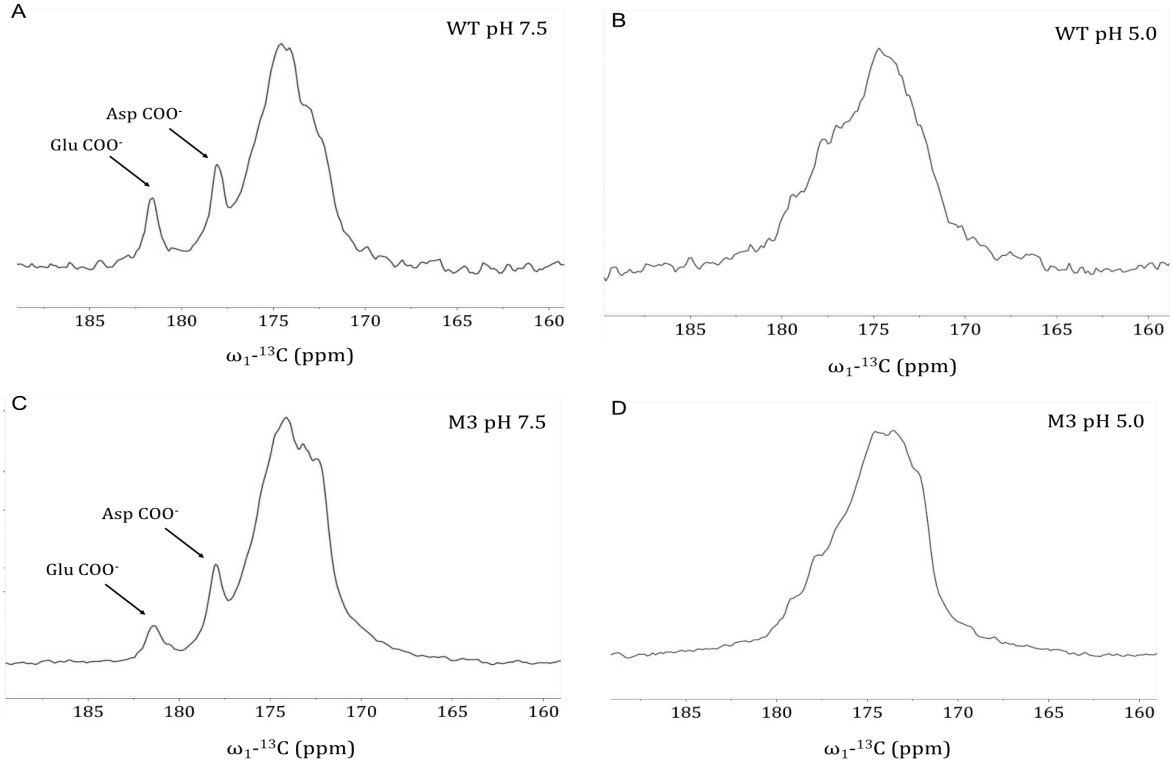

Figure 3. 1D ^{13}C-DP MAS NMR spectra of wild-type PsbS (A and B) and M3 E69Q/E176Q mutant (C and D) at pH 7.5 (A, C) and pH 5.0 (B, D) conditions.

PsbS pH-dependent secondary structure conformational changes: Fourier Transform infrared (FTIR) spectroscopy

To explore the possibility of a secondary-structure response of PsbS to a change in pH, we performed FTIR and 2D infrared (2DIR) spectroscopy in the Amide I region. The Amide I bands arise mainly from C=O oscillators in the protein backbone, and their frequencies are sensitive to particular secondary structure elements (α-helix, β-sheet and loops/turns) and their microenvironment, e.g. the degree of solvent exposure. The spectra were collected in D_2O detergent buffer solution rather than H_2O to avoid the O-H bend absorption which overlaps with Amide I. For this reason, the description of the FTIR results will be conducted in terms of pD rather than pH. Fig. 4 shows the FTIR spectra of wild-type PsbS

and of the three mutants at pD 7.5 (orange lines) and pD 5.0 (green lines) conditions, together with the difference spectrum of pD 5.0 minus pD 7.5 (black lines). The wild type FTIR spectrum at pD 7.5 (Fig. 4A, orange line) shows that the Amide I band is centered at 1640 cm^{-1} with a broad shoulder at frequencies up to 1690 cm^{-1}, indicative of predominant helical and loop contributions [26], consistent with the X-ray structure [19] and CD data [24]. Importantly, the spectrum contains a sharp band at 1630 cm^{-1} that will be discussed in detail below. In addition, the pD 7.5 FTIR spectrum shows a prominent band at 1550 cm^{-1} that originates from deprotonated carboxylic acid (the COO^- stretch mode), representative of deprotonated Glu and Asp residues [27]. In the spectral region around 1550 cm^{-1}, also the Amide II mode is expected to contribute, which arises from the backbone C=N stretch coupled to the amide N-H bend. However, because the protein has been dissolved in D_2O, the Amide II band is downshifted by 100 cm^{-1} [28] to ~1450 cm^{-1}, outside of the probed spectral window.

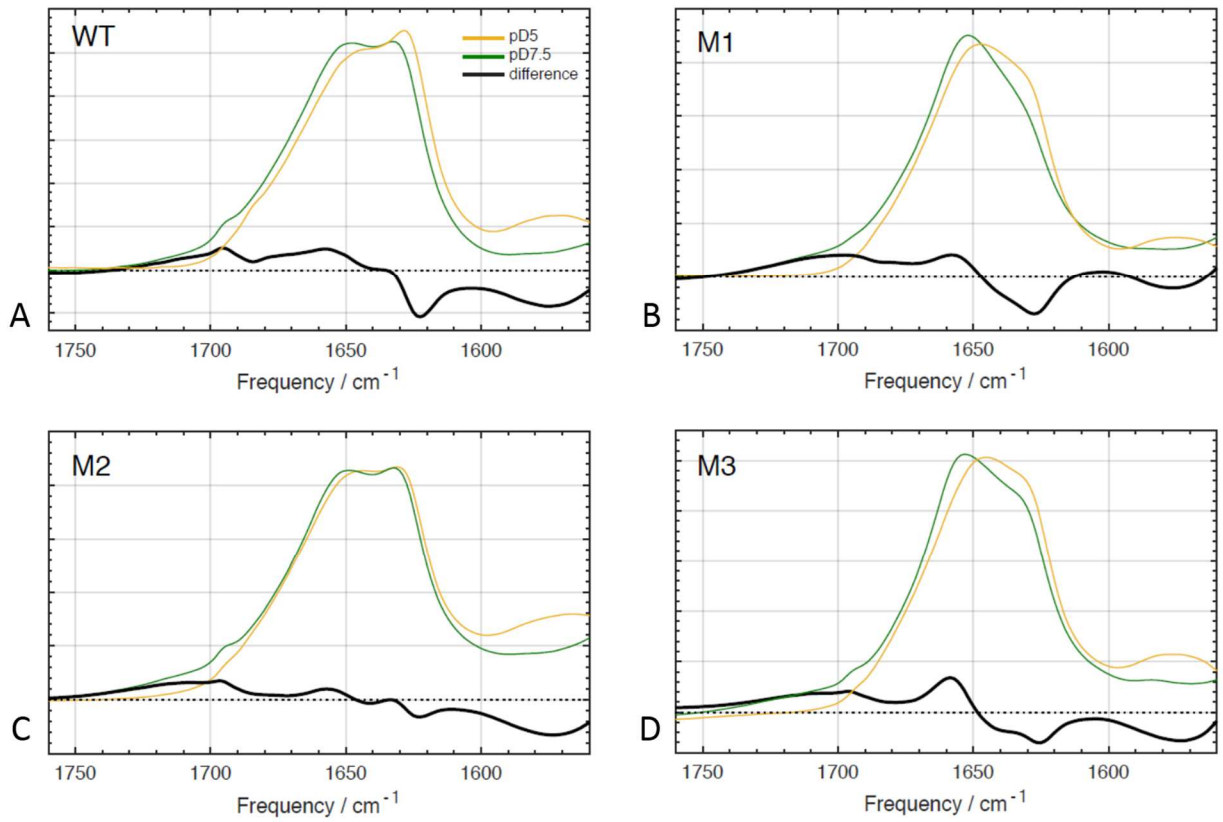

Figure 4. FTIR spectra of A: wild-type PsbS; B: M1 (E71Q) mutant; C: M2 (E176Q) mutant and D: M3 (E71Q / E176Q) mutant at pD 7.5 (orange) and pD 5.0 (green) and the difference spectra of pD 5.0 minus pD 7.5 (black). All spectra were taken in D_2O buffer.

Significant changes are observed in the FTIR spectrum for wild-type PsbS at lower pD. At pD 5.0 (Fig. 4A, green line), the 1550 cm^{-1} band is entirely absent while a new shoulder from ~1700 to 1750 cm^{-1} is observed, indicative of protonated (or in this case, deuterated) carboxyls (COOH) [27]. This observation demonstrates that all Glu and Asp are protonated at this pH, in agreement with the NMR results (Fig. 3B and D). In addition to the protonation effects, the pD 5.0-minus-pD 7.5 difference spectrum exhibits changes in the Amide I region from 1610 to 1690 cm^{-1}. It shows a negative sharp signal at 1625 cm^{-1} and a broad, positive band centered at 1660 cm^{-1}, which may be assigned a change in the Amide I band, and hence to conformational changes in the PsbS secondary structure. The integrated bleach amplitude of the

1625 cm^{-1} band corresponds to 3.6% of the integrated Amide I absorption, and with a total of 221 amino acids in *P. patens* PsbS plus the 6-His tag, hence involves at least 8 amino acid backbone oscillators.

In contrast to the wild type spectrum, in the FTIR spectrum of the M2 mutant only small changes are observed comparing the two pD conditions, with a minor negative band at 1625 cm^{-1} and a small positive absorption around 1658 cm^{-1} in the difference spectrum (Fig. 4C, black line). Yet, the deprotonated carboxyl signals at 1550 cm^{-1} (negative) and the protonated carboxyl signals at 1700 – 1750 cm^{-1} (positive) have been conserved as compared to wild type, indicating that the Glu/Asp protonation states have not been significantly altered with respect to the wild type. This observation indicates that protonation of Glu-2 (E176) specifically triggers the backbone conformational changes in wild type PsbS on lowering the pD from 7.5 to 5.0. Notably, the Amide I spectra of M2 under both pD conditions are similar to that of the wild type at low pD (Fig. S1).

The Amide I spectra of M1 and M3 mutant (Fig. 4B, D, respectively) do not resemble the wild type spectra at either pD conditions, consistent with the fact that the NMR carbonyl spectrum of the M3 differed from that of the wild type at both pH conditions. In particular, the prominent band around 1630 cm^{-1} that is conspicuously present in wild type at pD 7.5, and to a lesser extent at pD 5.0, and in the M2 mutant at both pD conditions, is largely absent. We conclude that mutation of Glu-1 (E71) significantly affects the secondary structure of PsbS. The difference spectra of M1 and M3 in the Amide I region show a well-resolved positive band at 1660 cm^{-1} and negative signal intensities between 1625-1640 cm^{-1}. The difference spectrum of M3 shows that if both active Glu are mutated, conformational changes occur that are not present in the wild type and that must be induced by protonation of other protonable residues at low pH. Indeed, both the IR and NMR data indicate that going from pH 7.5 to pH 5.0, all the protonable Asp and Glu residues undergo a change in protonation state. However, given that the secondary structures of the M1 and M3 mutants significantly differ from the wild-type structure, these changes are likely unrelated to the native PsbS response to pH and it is not feasible at this point to assign these structural changes to any active site in the protein.

PsbS pH-dependent secondary structure conformational changes: 2DIR spectroscopy

The FTIR results clearly indicate specific conformational changes in the PsbS secondary structure, but they are ambiguous with respect to the type of secondary structure element (i.e., helix, sheet of loop/coil) that undergoes a change or is newly formed. In particular, the negative feature at 1625 cm^{-1} might correspond to either β-sheet or α-helix, and the positive feature at 1660 cm^{-1} could correspond to a helix or a coil/loop [26]. To resolve any ambiguities, we applied two-dimensional IR spectroscopy (2DIR) to PsbS, which has a larger resolving power in this regard. The steady-state 2DIR spectrum of wild-type PsbS at pD 7.5 taken at a population time T = 400 fs is presented in Fig. 5A, with the excitation frequency Ω_{exc} along the vertical axis and the emission frequency Ω_{emis} along the horizontal axis. The linear FTIR spectrum is shown in the upper panel, reproduced from Fig. 4A. The 2DIR spectrum exhibits spectral congestion as typically observed in several other protein systems due to the overlapping Amide I contributions of several structural elements [29]. Adjacent to the negative bleach bands along the diagonal, reflecting depopulation of ground state modes $v = 0 \longrightarrow 1$, we observed corresponding anharmonic satellite peaks of positive sign, corresponding to the $v = 1 \longrightarrow 2$ transition and slightly red-shifted along Ω_{emis}.

We recorded 2DIR spectra at pD 5.0 and pD 7.5, and determined the difference spectrum (Fig. 4B), thereby scaling the 2DIR spectra on the integrated linear Amide I absorption between 1610 and 1690 cm^{-1} of both samples. We applied this procedure because the 2DIR signal scales with the 4th power of the transition dipole moment [30], and hence the 2DIR spectrum can potentially give a nonlinear amplitude response upon conformational change. The FTIR difference spectrum is shown in the upper panel. The 2DIR difference spectrum shows significantly less spectral congestion as several discrete peaks are observed, indicating that specific conformational changes take place as a function of pD. Beginning on the low frequency side, there is a $v = 0 \longrightarrow 1$, $v = 1 \longrightarrow 2$ positive/negative peak pair centered at ~1630 cm^{-1}, nearly coinciding with the negative feature identified in the difference FTIR spectrum at 1625 cm^{-1}. Accordingly, the sign of the 1630 cm^{-1} band in 2DIR is positive, reflecting population loss with the

positive lobe falling on the diagonal. This signal thus represents loss (or rather rearrangement, as we will see below) of a specific secondary structure element. Two diagonal peak pairs of opposite sign with respect to that at 1630 cm^{-1} are located at 1638 and 1660 cm^{-1}, i.e. with a negative amplitude on the diagonal, which indicates that these pairs represent population gain of two distinct secondary structure elements. The 1660 cm^{-1} band has an amplitude that is slightly (~30%) higher than that at 1638 cm^{-1}. A strong cross peak [1630,1665] lies between the highest and lowest diagonal bands.

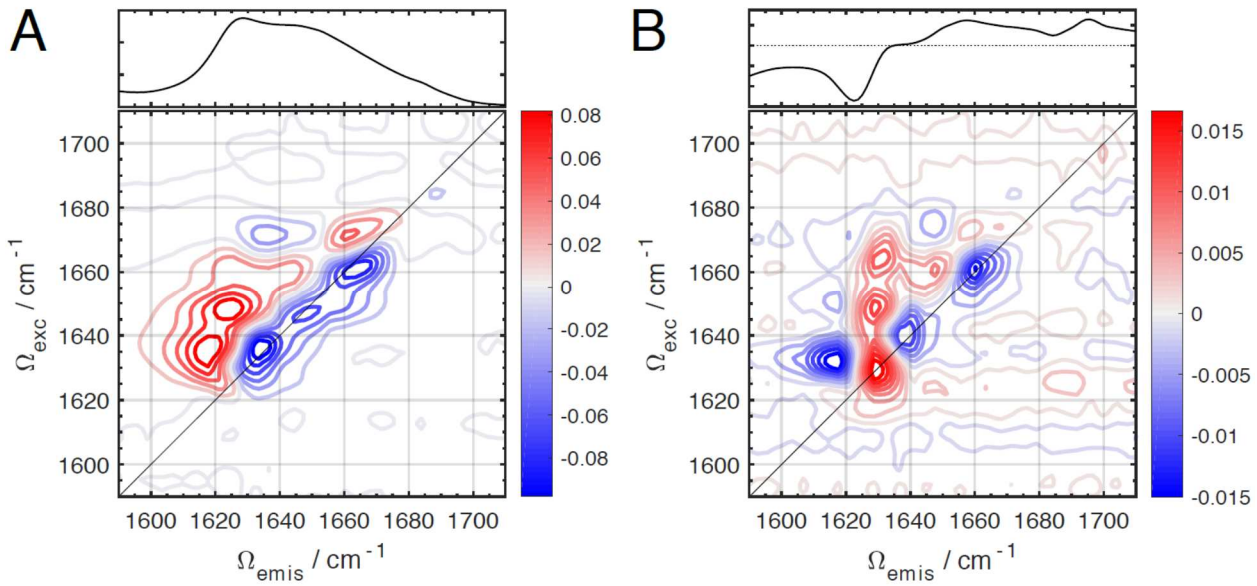

Figure 5. A: Steady-state 2DIR correlation spectrum at T=400 fs of wild-type PsbS in pD 7.5 buffer. B: pD 5.0 – pD 7.5 difference 2DIR of wild-type PsbS.

The nature of the 1630 cm^{-1} transition warrants further attention since this frequency falls on the boundary expected for α-helical and β-sheet amide I oscillators [26]. The band anharmonicity Δ of the 1630 cm^{-1} transition, i.e., the difference of the $v = 0 \longrightarrow 1$ and $v = 1 \longrightarrow 2$ peak maxima, amounts to $\Delta = 13$ cm^{-1}. This observation implies that it corresponds to an ordered secondary structure element, as Δ inversely scales with the degree of excitonic coupling between the Amide I oscillators [31], and uncoupled Amide I

oscillators give Δ values of 16 cm^{-1} [32]. β-sheets exhibit a characteristic "Z-shaped" 2DIR peak pattern [33] which is not observed here, and we hence conclude that the 1630 cm^{-1} feature corresponds to loss of a helical element. This agrees with the X-ray structure and CD data of PsbS which indicate no extensive β-sheet content [19,24]. A similar reasoning may be applied to the two band pairs at 1638 and 1660 cm^{-1}, which show band anharmonicity similar to that at 1630 cm^{-1}, no Z-shape 2DIR pattern and thus indicate gain of two distinct helical elements. Notably, the combined negative amplitudes along the diagonal of the 1638 and 1660 cm^{-1} bands are similar to that of the diagonal positive amplitude at 1630 cm^{-1}.

Comparing the 2DIR spectra with the FTIR spectra, the positive 1630 cm^{-1} band in 2DIR clearly corresponds with the negative 1625 cm^{-1} band in FTIR, while the negative band at 1660 cm^{-1} in 2DIR corresponds to the positive 1660 cm^{-1} band in FTIR. The positive 1638 cm^{-1} band in 2DIR is not clearly resolved in the FTIR spectrum, yet the latter shows a positive-going amplitude shoulder at 1638 cm^{-1} that is apparently superimposed on the 1625 cm^{-1} bleach. This explains the 5 cm^{-1} difference in the respective band amplitude maxima in 2DIR (1630 cm^{-1}) and FTIR (1625 cm^{-1}), which likely results from compensation by positive signals at 1638 cm^{-1} at the high-frequency side in the FTIR difference spectrum, as can also be deduced from the asymmetric lineshape of the 1625 cm^{-1} bleach (Fig 4A).

In addition to the diagonal peaks discussed above, the 2DIR difference spectrum features a prominent [1630,1665] cross peak. In general, cross peaks arise when specific oscillators with distinct frequencies are anharmonically coupled; such may occur through-bond or through-space. The [1630,1665] cross peak vertically aligns with the 1630 cm^{-1} diagonal band, suggesting that it originates from this helical element that exists at pD 7.4 and disappears at pD 5.0. The cross peak does not align horizontally with the 1660 cm^{-1} diagonal band in the difference spectrum, indicating that it is likely unrelated to the structural element at that frequency that arises at pD 5.0. Most likely, the cross peak results from a loss of coupling upon lowering the pD between the helical element that exists at pD 7.5 with adjacent Amide I elements that absorb at 1665 cm^{-1}.

An additional useful means to gain molecular insight from 2DIR spectroscopy lies in the slope of the nodal line (NLS) between the $v = 0 \longrightarrow 1$ and $v = 1 \longrightarrow 2$ transitions. This quantity is proportional to the vibrational energy gap frequency-frequency correlation function (FFCF) and reports on the degree of vibrational inhomogeneity of the system [34-36]. We calculated the NLS of each diagonal band pair by applying a linear fit to the zero crossing (nodal line) within the FWHM of each peak. The band pair at 1630 cm^{-1} has a NLS nearly parallel to the Ω_{exc} axis, as illustrated in Fig. S2, which indicates a highly homogeneous structure. In contrast, the band at 1638 cm^{-1} has a NLS nearly parallel to the diagonal, representing a case with large heterogeneity. The 1660 cm^{-1} band pair demonstrates a NLS in between the former examples, which can be interpreted as a case with intermediate heterogeneity.

Our interpretation of the pD 5.0 minus pD 7.5 difference 2DIR results, considering their frequency, anharmonicity, inhomogeneity, and sign, is as follows:

i) the 1630 cm^{-1} diagonal peak reflects loss of a single well-ordered helical element in a homogeneous environment and corresponds to the negative signal observed in the difference FTIR spectra. The low frequency of 1630 cm^{-1} of this helical element indicates that it has a high degree of exposure to the aqueous solvent [37,38].

ii) the minor 1638 cm^{-1} diagonal peak represents gain of a helical element that exhibits a significant degree of conformational disorder.

iii) the major 1660 cm^{-1} diagonal peak represents gain of a helical element with an intermediate degree of conformational disorder.

iv) Given that the combined amplitudes of the 1638 and 1660 cm^{-1} diagonal bands are similar to that of the corresponding band at 1630 cm^{-1}, we conclude that the helical content remains approximately the same at the two pD conditions. Hence, no significant unfolding, which would result in lowering of the 2DIR amplitude [30], takes place.

Discussion

Monomer/dimer content of wild-type and mutant PsbS

To interpret the observed pH-dependent changes observed in wild-type PsbS and the M1, M2 and M3 mutants, we turn to the crystal structure of spinach PsbS, which represents PsbS at low pH [19]. In the crystal structure, Glu-1 (E69 in the X-ray structure) is located in a luminal loop that connects two transmembrane helices TM1 and TM2, whereas Glu-2 (E173 in the X-ray structure) is located in the amphipathic short helix H2 at the water-membrane interface facing the lumen, and connects TM3 and TM4 (Fig. 1). In the PsbS structure, the backbone carbonyl and side chain carboxyl of Glu-2 each can form a hydrogen bond with two backbone amides of I74 and Y75 in the luminal loop of the adjacent monomer as shown in Fig. 6C. The residues I74 and Y75 are part of a short 3-10 helix fragment. In *P. patens* PsbS, the latter two amino acids are L74 and T75. Fig.6D shows a schematic picture of dimer-stabilizing interactions at the luminal side. At the luminal side, the dimer is stabilized by four hydrogen bonds, connecting Glu-2 in the amphipatic helix H2 (E173 or E176 in *spinach*, resp. *P. patens* PsbS) of monomer 1 to the luminal loop, which contains Glu-1 (E69 or E71 in *spinach*, resp. *P. patens* PsbS) of monomer 2 and *vice versa*.

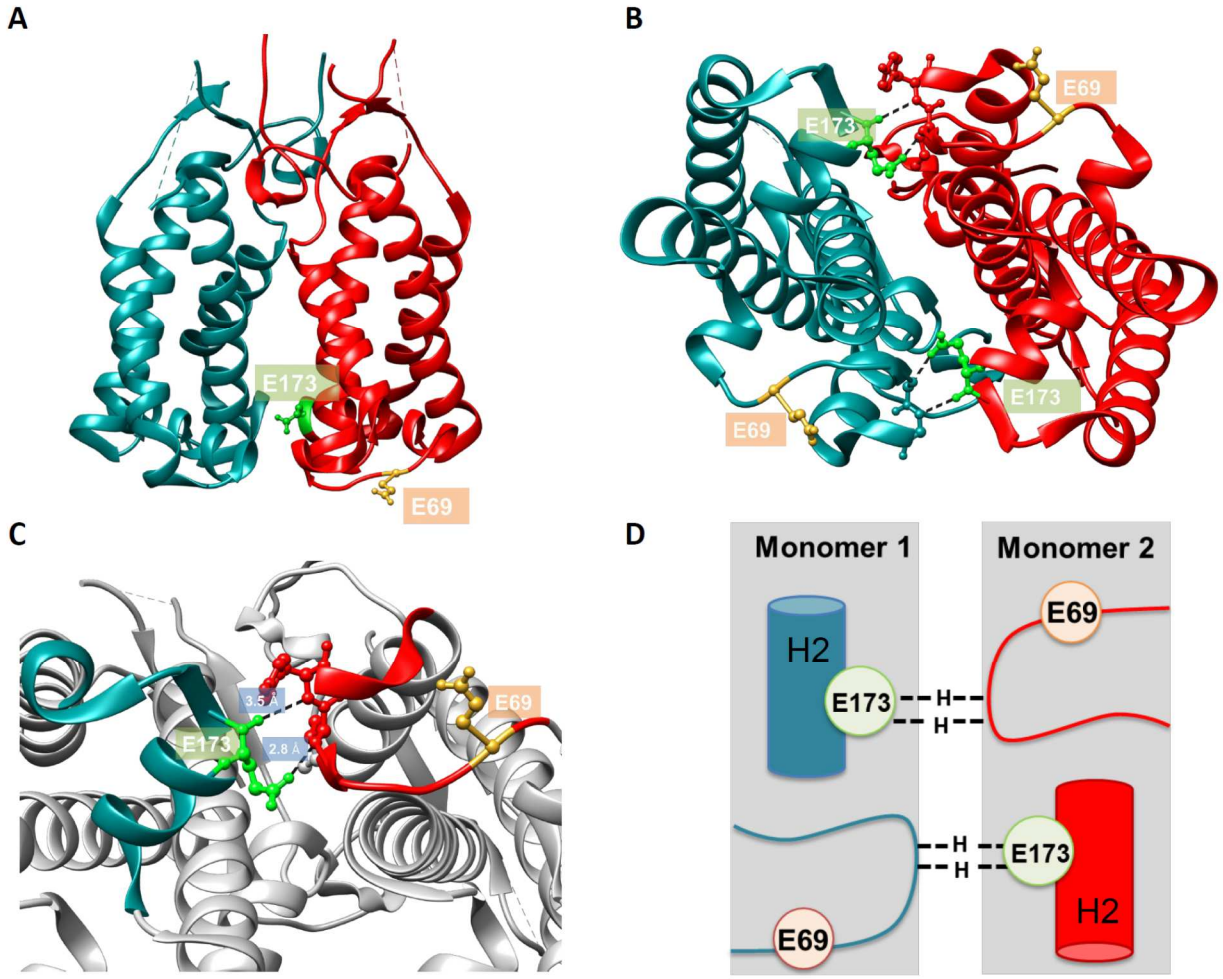

Figure 6. A: PsbS dimer (*PDB-ID 4RI2* [19]) with the two active Glu-1 (E69, in yellow) and Glu-2 (E173, in green); B: lumen view, showing the inter-monomer H-bonds formed by Glu-2 (E173); C: close-up of helix H2 containing Glu-2 (E173) connecting to the lumen loop containing Glu-1 (E69) of the adjacent monomer and D: schematic picture of the inter-monomer stabilizing interactions at the lumen site, involving Glu-2 (E173) in helix H2 and the lumen loop containing Glu-1 (E69).

The M1 mutant is strongly impaired in dimerization (Fig. 2B), even though Glu-1 is not close to the dimer interface and in fact, is at the exterior side of the PsbS dimer as shown in Fig. 6A and B. Yet, as we mentioned, this residue is part of the luminal loop that is connected to Glu-2 of the adjacent monomer via two hydrogen bonds. The highly reduced dimer content of M1 at acidic and neutral pH conditions

suggests that the site of Glu-1 has an allosteric effect on the dimerization of PsbS. Possibly, substitution of this residue by Gln may re-orient the luminal loop, disrupting the inter-monomer hydrogen bonds to Glu-2.

The M2 mutant is still capable of dimer formation, even though this mutant lacks Glu-2 that is involved in forming two inter-monomer hydrogen bonds to two amide NH groups of the adjacent monomer (Fig. 6C,D). This can be explained since in the M2 mutant, Glu-2 is substituted by Gln, which contains a side chain carbonyl that is equally capable of receiving a hydrogen, whilst the H bond involving the Glu-2 backbone carbonyl can equally be formed by the Gln backbone carbonyl.

Assignment of wild type PsbS conformational changes to re-positioning of amphipatic helix H2

We now discuss the origin of the Amide I difference signals observed in FTIR and 2DIR spectroscopy, which indicate conformational changes in the secondary structure. In FTIR, we observe a distinct negative/positive Amide I signal at 1625 (-) / 1660 (+) cm^{-1} , and a positive-going shoulder at 1638 cm^{-1} in WT PsbS (Fig. 4A). This signal is also reflected and refined in 2DIR spectroscopy, where loss of a helical signal at 1630 cm^{-1} is accompanied by gain of two distinct helical signals at 1638 cm^{-1} and 1660 cm^{-1} at comparable amplitude (Fig. 5B). Strikingly, mutation of M2 almost completely abolishes the structural Amide I response of PsbS to low pH (Fig. 4C). This observation reveals that the lumen-facing amphipatic helix H2 that contains Glu-2 (see Fig. 1) likely represents the site of plasticity that undergoes a pH-dependent structural change and is responsible for the characteristic FTIR and 2DIR signals. This assignment is consistent with the FTIR amplitude of the difference signal in WT PsbS, which corresponds to at least 8 amino acids, which agrees with the length of the H2 helix in the X-ray structure, 9 amino acids [19]. It must be noted that the 1625 cm^{-1} signal is partly compensated by a positive signal at 1638 cm^{-1}, which implies that the number of involved amino acids probably is somewhat larger than 8.

Because Glu-2 is negatively charged at neutral pH, it is expected that at pH 7.5, the polar side of the amphipatic helix H2 will be stabilized at the aqueous environment of the lumen, consistent with the

low frequency (1630 cm^{-1}) of the helical element detected at that pH (pD). At pH (pD) 5.0, two populations of helical elements were detected with comparable amplitudes, with frequencies of 1660 and 1638 cm^{-1}. The helical signal at 1660 cm^{-1} clearly indicates a hydrophobic environment. We therefore propose that protonation of Glu-2 at low pH causes the H2 helix to re-position from the aqueous phase into the membrane phase, as schematically illustrated in Fig. 7. The 1638 cm^{-1} helical signal detected at pH (pD) 5.0 indicates a remaining degree of solvent exposure, suggesting that a fraction of the H2 helices undergoes incomplete movement into the hydrophobic phase. The observation of this incompletely moving fraction of H2 helix may relate to the less-well defined demarcation between aqueous and hydrophobic phase in detergent micelles as compared to a lipid bilayer environment.

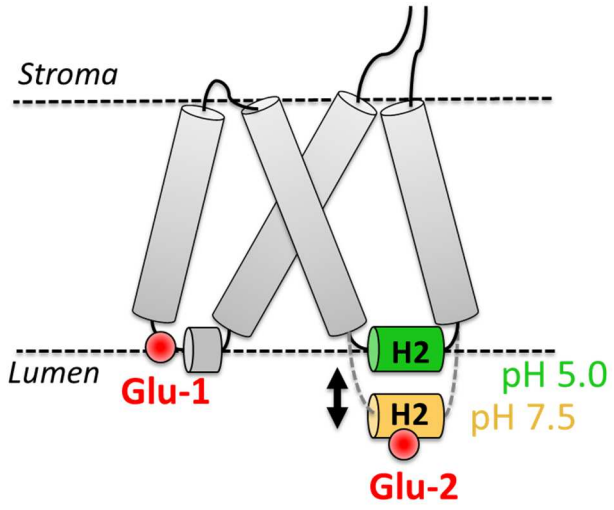

Fig. 7: schematic illustration of the pH-dependent movement of helix H2 in PsbS.

The idea of helix H2 re-positioning into the membrane phase at low pH is consistent with low-pH crystal structures obtained from crystals that were soaked with *N,N'*-Dicyclohexylcarbodiimide (DCCD), a hydrophobic compound that binds to carboxyl groups of protonated amino acids that are shielded from aqueous environments. The DCCD was used to detect protonation sites of PsbS in the crystal structure [19]. The DCCD-soaked structure shows that DCCD binds to Glu-2 (E173), indicating that in the low-pH conformation, this Glu residue indeed resides in a hydrophobic environment [19].

According to the 2DIR difference spectrum (Fig. 5B), helix H2 is in a highly ordered, homogenous state at neutral pH, as judged from the nodal line slope (NLS). At low pH, helix H2 shows an increased inhomogeneity, from which we conclude that H2 re-positioning from the aqueous phase into the membrane phase is accompanied by increased conformational freedom of this protein fragment.

Possibly, the displacement of helix H2 causes a change of hydrogen bond interactions with the loop containing Glu-1 that connect TM1 and TM2 (Fig. 6), which in turn may affect the PsbS monomer/dimer equilibrium. The wild-type PsbS has somewhat larger dimer content on gel at low pH, which suggests that re-positioning of H2 into the hydrophobic phase strengthens the inter-monomer hydrogen bonding interactions. Results from our previous work suggested that dimer contents of PsbS in detergent solutions changed over time, and in fact it was observed that after several days the dimer content would be larger at neutral pH than at low-pH solutions [24]. Here, the analysis was performed on freshly prepared samples. From molecular-dynamics (MD) simulations, it has been proposed that at high pH, hydrogen bonds are formed between E173 and T162 of the adjacent monomer that are destabilized at low pH [39]. In this light, re-positioning of H2 at low pH may strengthen specific hydrogen-bond interactions while weakening others, delicately controlling the stability of PsbS dimers.

In the M2 mutant, the charge at the Glu-2 site is neutralized by the Glu to Gln mutation, which predicts that M2 PsbS will already adopt a low-pH conformation at neutral pH. This is exactly what is observed, since the Amide I FTIR spectrum of M2 at both pH conditions resembles the low-pH spectrum of the WT (Fig. S1).

The IR spectrum of M1 does not resemble the wild-type IR spectrum at low or neutral pH, indicating that part of the M1 PsbS mutant adopts a non-native fold. The luminal loop containing Glu-1 contains an additional conserved, second Glu close to TM2 (E76 for *spinach* PsbS and E78 for *patens* PsbS), and, for *P. patens* PsbS, also contains an Asp residue (D69). At neutral pH, those residues will have a negative charge, while in M1 and M3 the Glu-1 site is neutralized by Gln replacement, resulting in a charge distribution along the luminal loop stretch that neither reflect the luminal loop charges of wild-type

PsbS at neutral pH, nor reflects the loop charges of the wild type at low pH conditions. This may lead to a non-native fold of the luminal loop stretch in M1 and M3, accounting for the difference in secondary structure compared to the WT. The collective effect of Glu-1 and Glu-2 mutation may produce a moderated PsbS structure, in which the substituted Gln at the Glu-2 helix site is capable of interacting with the modified loop of the adjacent monomer, which could explain why dimers are more stabilized in M3 than in M1.

Conclusions

Summarizing, we discovered that the two active Glu sites respond non-equivalently to lowering of the pH. The luminal loop containing Glu-1 has an allosteric effect on PsbS dimerization. Glu-2 is responsible for the structural response of PsbS to lowering the pH, most likely by a re-positioning of the amphipatic short helix fragment H2 from the aqueous phase into the membrane phase, thereby becoming less ordered. Single-point mutations of Glu-1 and Glu-2 in PsbS have been reported to severely reduce NPQ activity [20], implicating that both dimerization and flexibility of the amphipathic short helix stretch H2 are important for PsbS function. The M2 mutant represents the low-pH state of PsbS, which is the active state. Reduced NPQ activity of this mutant in plants suggests that not the activation of PsbS, but its ability to switch on and off is crucial for its function. Indeed, PsbS is not only involved in switching on NPQ, but also essential for rapid de-activation and recovery of this process in fluctuating light conditions [21].

The question that now arises concerns the relation of the pH-dependent H2 helix displacement with the PsbS functional switch and the next challenge will be to relate the conformational switch to the PsbS function *in vivo* in interaction with key constituents of the thylakoid membrane. PsbS is a member of the LHC superfamily, of which proteins form pH switches (namely PsbS and LHCSR) and/or photoprotective switches that can alternate between fluorescent and excitation-quenched states (namely LHCII and LHCSR). LHCs share a structure in which transmembrane helices are connected via amphipatic short helices at the luminal site [40-43]. Responsiveness of the amphipatic helices to changes in

pH, hydrophobicity or other alterations in the physico-chemical environment might be a common motif that enables LHCs to operate as molecular controls for regulating photosynthetic light harvesting.

Materials and Methods

Construction of mutants, protein expression, refolding and purification

Constructured plasmids of site-directed mutants of *P. patens* PsbS were purchased from Baseclear B.V.® . Single mutants were constructed in which E71 was replaced by Q (E71Q) or E176 was replaced by Q (E176Q) that are referred to as M1 and M2 respectively. A double mutant in which both E71 and E176 were mutated to Q (E71Q/E176Q) was constructed and is referred to as M3. The mutant *patens* PsbS genes were inserted into a pExp5-vector containing an N-terminal His_6-tag. The plasmids were transformed, and the mutant proteins were overexpressed in *E. coli* and purified as has been described for wild-type PsbS in [24]. Wild-type and mutant PsbS were refolded in *n*-Dodecylphosphocholine (FC-12) detergent buffers at pH 5.0 and pH 7.5 conditions, using 100mM sodium acetate (pH 5.0) or sodium phosphate (pH 7.5) buffers. For the NMR experiments, ^{13}C and ^{15}N uniform labelling of PsbS WT and M3 mutant was carried out by protein overexpression using standard minimal media containing ^{13}C-glucose and ^{15}N-ammonium chloride. For the FTIR and 2DIR experiments, the proteins were prepared in deuterated detergent buffer equilibrated at pD 7.5 or pD 5.0.

Sodium dodecyl sulfate (SDS)-page gel electrophoresis

SDS-page gel electrophoresis analysis (12.5% running gel, 4% stacking gel stained with Coomassie brilliant blue R-250 Bio-Rad) was carried out for checking the yield of PsbS at every step of overexpression, purification and refolding. For staining, 2.5µL of Precision Plus Protein™ Dual Color Standard from Sigma was used.

NMR spectroscopy

Solid-state NMR measurements were performed on a Bruker Avance I 750-MHz wide-bore solid-state NMR spectrometer with 17.6 Tesla magnetic field. In this field, ^{13}C and ^{1}H resonate at 188.66 and 750.23 MHz respectively. Standard 4 mm triple resonance MAS probe was used. All the samples were packed in 4mm zirconium rotors with top insert and were spun at the magic angle (54.74^0). The spinning frequency was set at 13 kHz. The temperature was set at 293 K. ^{13}C spectra were obtained through direct polarization also referred to as 'hpdec'. 90^0 or ($\pi/2$) carbon pulses of 6.2 µs and 3.1 µs proton pulses were applied. An acquisition time of 36.2 ms was used. For the experiments, 1024 scans were acquired with a constant recycle delay of 5 s. A line broadening function of 50 Hz was applied for processing the spectra. All the ^{13}C spectra were externally referenced to methyl signal of tetramethylsilane (TMS).

FTIR spectroscopy

Infrared difference spectra were recorded using an FTIR spectrometer (IFS 66s Bruker) equipped with a nitrogen-cooled photovoltaic Mercury Cadmium Telluride (MCT) detector (20 MHz, KV100, Kolmar Technologies) described earlier [44,45]. The samples were contained between CaF_2 windows separated with a 20 µm Teflon spacer and the concentration was tuned for OD ~0.8 absorption at 1650 cm^{-1}. The measurements were carried out at room temperature and spectral resolution of the instrument was 3 cm^{-1}. The samples were solubilized in D_2O detergent buffer at either pD 5.0 or pD 7.5.

2DIR spectroscopy

Two-dimensional infrared spectroscopy (2DIR) was carried out in the pump-probe geometry as previously described [46,47], as an extension to an existing femtosecond mid-IR spectrometer [48]. In short, femtosecond midIR pulses were generated via difference frequency generation in Ag_2GaS_2 (100 fs pulse duration, 200 cm^{-1} bandwidth) pumped by a Ti:sapphire regenerative amplifier with 1 kHz repetition rate. A 5% fraction was split off for the probe beam with a wedged CaF_2 window. The pump beam was

modulated with a germanium acousto-optic modulator (Quickshape, Phasetech, Madison WI). Data was collected in the time domain by oversampling along the free induction decay (τ) in the rotating frame with a two-pulse, four-frame phase-cycling scheme to isolate the $\chi^{(3)}$ response and remove contributions from scattered pump light *in situ*. The pump and probe beams were focused on the sample with an off-axis parabolic mirror, overlapped in space, and set to a designated delay using a motorized linear delay stage. The transmitted probe beam was collimated and detected with a 64-element Mercury Cadmium Telluride (MCT) photodiode array (Infrared Associates). A parallel polarization condition <ZZZZ> was employed by tuning the polarization of the pump beam with a combination $\lambda/2$ MgF_2 waveplate (Karl Lambrecht) and wire-grid polarizer (Thorlabs). The PsbS samples were contained between two CaF_2 windows separated with a 20 µm Teflon spacer. D_2O buffer solution was used to minimize the background absorption. Measurements with the pD 5.0 and 7.5 samples were collected consecutively and difference 2DIR spectra were produced by scaling according to the integrated linear absorption of the amide I band (1610 – 1690 cm^{-1}).

ASSOCIATED CONTENT

Supporting Information. Overlaid FTIR spectra of wild type and M2 mutant PsbS; nodal line slopes (NLS) for the diagonal bands in 2DIR.

AUTHOR INFORMATION

Corresponding Author

a.pandit@chem.leidenuniv.nl

j.t.m.kennis@vu.nl

ACKNOWLEDGMENT

Dr. Karthick Babu Sai Sankar Gupta is greatly acknowledged for assistance with the NMR spectroscopy. This work was supported by the Chemical Sciences Council of the Netherlands Organization for Scientific Research (NWO-CW) through a VICI grant to J.T.M.K (nr. 724.011.004). and an NWO-CW VIDI grant to A.P. (nr. 723.012.103).

REFERENCES

(1) Ruban, A. V.; Johnson, C. D. P.; Duffy *Biochimica et biophysica acta. Bioenergetics* **2012**, *1817*, 167.

(2) Croce, R.; van Amerongen, H. *Nature Chemical Biology* **2014**, *10*, 492.

(3) Niyogi, K. K.; Truong, T. B. *Current Opinion in Plant Biology* **2013**, *16*, 307.

(4) Engelken, J.; Funk, C.; Adamska, I. *The Extended Light-Harvesting Complex (LHC) Protein Superfamily: Classification and Evolutionary Dynamics*, 2011; Vol. 33.

(5) Funk, C.; Adamska, I.; Green, B. R.; Andersson, B.; Renger, G. *The Journal of biological chemistry* **1995**, *270*, 30141.

(6) Goral, T. K.; Johnson, M. P.; Duffy, C. D. P.; Brain, A. P. R.; Ruban, A. V.; Mullineaux, C. W. *The Plant Journal* **2012**, *69*, 289.

(7) Ikeuchi, M.; Uebayashi, N.; Sato, F.; Endo, T. *Plant and Cell Physiology* **2014**.

(8) Kiss, A.; Ruban, A.; Horton, P. *Journal of biological chemistry* **2008**, *283*, 3972.

(9) Ware, M. A.; Belgio, E.; Ruban, A. V. *Journal of Experimental Botany* **2015**, *66*, 1259.

(10) Wobbe, L.; Bassi, R.; Kruse, O. *Trends in Plant Science*, *21*, 55.

(11) Sylak-Glassman, E. J.; Malnoë, A.; De Re, E.; Brooks, M. D.; Fischer, A. L.; Niyogi, K. K.; Fleming, G. R. *Proceedings of the National Academy of Sciences* **2014**, *111*, 17498.

(12) Correa-Galvis, V.; Poschmann, G.; Melzer, M.; Stühler, K.; Jahns, P. *Nature Plants* **2016**, *2*, 15225.

(13) Dall'Osto, L.; Cazzaniga, S.; Bressan, M.; Paleček, D.; Židek, K.; Niyogi, K. K.; Fleming, G. R.; Zigmantas, D.; Bassi, R. *Nature Plants* **2017**, *3*, 17033.

(14) Gerotto, C.; Franchin, C.; Arrigoni, G.; Morosinotto, T. *Plant Physiology* **2015**, *168*, 1747.

(15) Sacharz, J.; Giovagnetti, V.; Ungerer, P.; Mastroianni, G.; Ruban, A. V. *Nature Plants* **2017**, *3*, 16225.

(16) Park, S.; Fischer, A. L.; Steen, C. J.; Iwai, M.; Morris, J. M.; Walla, P. J.; Niyogi, K. K.; Fleming, G. R. *Journal of the American Chemical Society* **2018**, *140*, 11965.

(17) Daskalakis, V. *Physical Chemistry Chemical Physics* **2018**, *20*, 11843.

(18) Bergantino, E.; Segalla, A.; Brunetta, A.; Teardo, E.; Rigoni, F.; Giacometti, G. M.; Szabò, I. *Proceedings of the National Academy of Sciences of the United States of America* **2003**, *100*, 15265.

(19) Fan, M.; Li, M.; Liu, Z.; Cao, P.; Pan, X.; Zhang, H.; Zhao, X.; Zhang, J.; Chang, W. *Nature Structural &Amp; Molecular Biology* **2015**, *22*, 729.

(20) Li, X. P.; Gilmore, A. M.; Caffarri, S.; Bassi, R.; Golan, T.; Kramer, D.; Niyogi, K. K. *The Journal of biological chemistry* **2004**, *279*, 22866.

(21) Kromdijk, J.; Głowacka, K.; Leonelli, L.; Gabilly, S. T.; Iwai, M.; Niyogi, K. K.; Long, S. P. *Science* **2016**, *354*, 857.

(22) Glowacka, K.; Kromdijk, J.; Kucera, K.; Xie, J.; Cavanagh, A. P.; Leonelli, L.; Leakey, A. D. B.; Ort, D. R.; Niyogi, K. K.; Long, S. P. *Nature communications* **2018**, *9*, 868.

(23) Hubbart, S.; Smillie, I. R. A.; Heatley, M.; Swarup, R.; Foo, C. C.; Zhao, L.; Murchie, E. H. *Communications Biology* **2018**, *1*, 22.

(24) Krishnan, M.; Moolenaar, G. F.; Gupta, K.; Goosen, N.; Pandit, A. *Sci Rep* **2017**, *7*, 15200.

(25) Fritzsching, K. J.; Yang, Y.; Schmidt-Rohr, K.; Hong, M. *Journal of biomolecular NMR* **2013**, *56*, 155.

(26) Krimm, S.; Bandekar, J. *Advances in Protein Chemistry* **1986**, *38*, 181.

(27) Barth, A. *Prog. Biophys. Mol. Biol.* **2000**, *74*, 141.

(28) Blout, E. R.; Deloze, C.; Asadourian, A. *Journal of the American Chemical Society* **1961**, *83*, 1895.

(29) Ganim, Z.; Chung, H. S.; Smith, A. W.; Deflores, L. P.; Jones, K. C.; Tokmakoff, A. *Accounts of Chemical Research* **2008**, *41*, 432.

(30) Dunkelberger, E. B.; Grechko, M.; Zanni, M. T. *Journal of Physical Chemistry B* **2015**, *119*, 14065.

(31) Zhao, J.; Wang, J. P. *Journal of Chemical Physics* **2012**, *136*.

(32) Wang, J. P.; Hochstrasser, R. M. *Journal of Physical Chemistry B* **2006**, *110*, 3798.

(33) Demirdoven, N.; Cheatum, C. M.; Chung, H. S.; Khalil, M.; Knoester, J.; Tokmakoff, A. *Journal of the American Chemical Society* **2004**, *126*, 7981.

(34) Eaves, J. D.; Loparo, J. J.; Fecko, C. J.; Roberts, S. T.; Tokmakoff, A.; Geissler, P. L. *Proceedings of the National Academy of Sciences of the United States of America* **2005**, *102*, 13019.

(35) Kwac, K.; Cho, M. H. *Journal of Chemical Physics* **2003**, *119*, 2256.

(36) Guo, Q.; Pagano, P.; Li, Y. L.; Kohen, A.; Cheatum, C. M. *Journal of Chemical Physics* **2015**, *142*.

(37) Byler, D. M.; Susi, H. *Biopolymers* **1986**, *25*, 469.

(38) Reisdorf, W. C.; Krimm, S. *Biochemistry* **1996**, *35*, 1383.

(39) Daskalakis, V.; Papadatos, S. *Biophysical Journal* **2017**, *113*, 2364.

(40) Standfuss, R.; van Scheltinga, A. C. T.; Lamborghini, M.; Kuhlbrandt, W. *Embo Journal* **2005**, *24*, 919.

(41) Li, X. P.; Bjorkman, O.; Shih, C.; Grossman, A. R.; Rosenquist, M.; Jansson, S.; Niyogi, K. K. *Nature* **2000**, *403*, 391.

(42) Pan, X. W.; Li, M.; Wan, T.; Wang, L. F.; Jia, C. J.; Hou, Z. Q.; Zhao, X. L.; Zhang, J. P.; Chang, W. R. *Nature Structural & Molecular Biology* **2011**, *18*, 309.

(43) Wei, X. P.; Su, X. D.; Cao, P.; Liu, X. Y.; Chang, W. R.; Li, M.; Zhang, X. Z.; Liu, Z. F. *Nature* **2016**, *534*, 69.

(44) Alexandre, M. T. A.; van Grondelle, R.; Hellingwerf, K. J.; Kennis, J. T. M. *Biophysical Journal* **2009**, *97*, 238.

(45) Toh, K. C.; Stojkovic, E. A.; Rupenyan, A. B.; van Stokkum, I. H. M.; Salumbides, M.; Groot, M. L.; Moffat, K.; Kennis, J. T. M. *Journal of Physical Chemistry A* **2011**, *115*, 3778.

(46) Shim, S.-H.; Strasfeld, D. B.; Ling, Y. L.; Zanni, M. T. *Proceedings of the National Academy of Sciences of the United States of America* **2007**, *104*, 14197.

(47) Shim, S.-H.; Zanni, M. T. *Physical Chemistry Chemical Physics* **2009**, *11*, 748.

(48) Konold, P. E.; Mathes, T.; Weissenhorn, J.; Groot, M. L.; Hegemann, P.; Kennis, J. T. M. *Journal of Physical Chemistry Letters* **2016**, *7*, 3472.